Ion acceleration and scattering by a collisionless shock wave

A. T. Altyntsev, G. N. Kichigin, N. V. Lebedev, and N. A. Strokin

Siberian Division, USSR Academy of Sciences

(Submitted 2 June 1988)
Zh. Eksp. Teor. Fiz. **96**, 574–582 (August 1989)

This study reports the experimental detection of a proton capture effect at the wave front of a transverse magnetoacoustic collisionless shock wave (CSW) and proton acceleration along the wave front due to resonant interaction with the electrostatic potential jump. The relationship between the reflected particles and those accelerated along the wave front is analyzed. The structural features of the ion beam reflected and scattered at a large angle are identified; such features are related to the appearance of two isomagnetic potential jumps at the front of the collisionless shock wave.

Nonthermal high-energy protons have been observed travelling normal to the plane of the wave front of a collisional shock wave (CSW) in experimental studies (for example in Refs. 1, 2); this has been attributed to their reflection by the electrostatic potential jump at the CSW wave front. Recently the mechansim of resonant charged particle acceleration along the CSW wave front ($U \times B$ acceleration) has been a subject of substantial interest to theoreticians. The trapped particles travelling with the wave transverse to the magnetic field are accelerated by the Lorentz force perpendicular to both the magnetic and radial electrical fields. Attention was first focused on this type of acceleration in Ref. 3. Subsequently this idea was developed in Refs. 4–6. Ionic acceleration by this mechanism has not yet been investigated experimentally.

The present study reports the experimental detection of resonant proton acceleration along a collisionless shock wave front in a plasma. The relationsip between particles travelling along the wave front and at angles of 90 and 35° to the wave front is analyzed.

1. DESCRIPTION OF THE EXPERIMENT

The experiment was carried out on a "UN-Phoenix" theta-pinch device. The initial plasma of density $n_0 = 4 \cdot 10^{12}$–$1.5 \cdot 10^{14}$ cm^{-3} was produced by pulsed injection of hydrogen to a quartz vessel 18 cm in diameter in a longitudinal (along the z axis) initial magnetic field of $B_0 = 200$–450 G. The magnetic field pulse of the piston B_1 was generated by means of a dual (primary and shorting) spark gap. The rise time of the field B_1 to the maximum value of 1100 G was 450 ns and the decay time to half amplitude was 3.5 μs. Application of the field would produce a cylindrical collisionless shock wave converging on the axis of the device.

The initial plasma density was monitored by means of a triple Langmuir probe. The radial magnetic field profile and shock wave propagation velocity U were measured by magnetic probes with an open loop 3 mm in diameter. The potential jump at the wave front was measured by floating electrical probes (potential probes) with $R_p = 12$ kΩ. Analogous probes with $R_p = 240$ Ω were used to monitor the "fast" potential profile. The temporal resolution of the entire recording circuit was better than 1 ns.

The ion energy spectra were reconstructed from the energy distributions of neutral charge-exchange particles. The measurments were carried out on an eight-channel energy analyzer in a 90–2000 eV energy range with an energy resolution $\Delta\varepsilon/\varepsilon = (33$–$4)\%$ and a temporal resolution 150–10 ns. The neutral particles were extracted from the working volume through a ceramic tube (aperture 10^{-4}) of which the intake used to analyze the particle acceleration dynamics along the CSW wave front was mounted at the point of tangency of the chords with circles of radius $r_1 = 3$ cm or $r_2 = 6$ cm. For transverse measurements of the wave front the tube was moved along the diameter past the axis of the device to radius r_1. The spectra of ions scattered in the r–φ lane were measured along a chord of radius r_1 for an angle $\alpha = 35°$ between the normal **n** to the wave front plane and the analyzer tube axis and in the r–z plane at an angle of 45°. The direction of the magnetic fields B_0 and B_1 was switched during the experiment in order to investigate the effect of the magnetic field sign (the direction of the induction electrical current at the CSW wave front) on energy acquired by the ions and to determine the degree of anisotropy of ion acceleration along the wave front.

2. EXPERIMENTAL RESULTS

2.1. Ion variations along the CSW wave front

Figure 1 provides sample signals from the magnetic probe $B_1(t)$ and from several energy analyzer channels $A_i(t)$ modified to account for the transit time between the

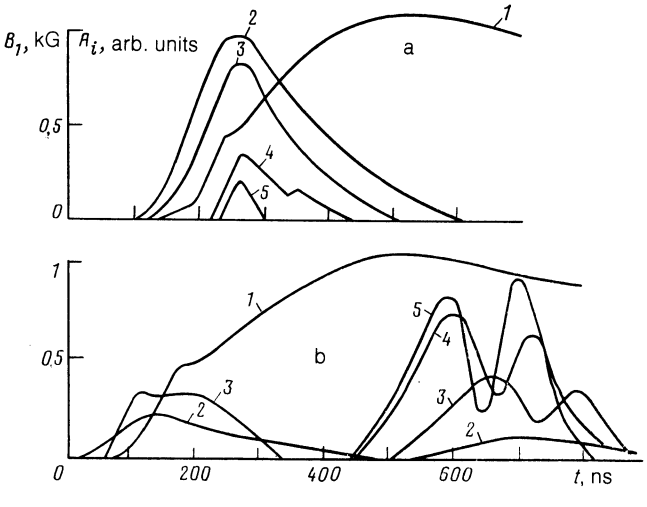

FIG. 1. Magnetic probe signals (1) and ion signals, taking into account the transient time between the tube point input and the detectors corresponding to particles of energies 190, 340, 930, 1120 eV (curves 2–5); $r_2 = 6$ cm, $B_0 = 212$ G, $n_0 \approx 3 \cdot 10^{13}$ cm^{-3}; a—backward, b—forward.

 0038-5646/89/080324-05$04.00

tube intake and the detector. The measurements were carried out for different current directions at the CSW wave front (the direction of positively charged particles was used as the current direction). We will refer to the case where the direction of ion motion along the CSW wave front is identical to the direction of the induced electrical current as the "forward" experimental formulation and will refer to the case where the direction of motion of the measured particles and the current are opposite as the "backward" formulation.

In the "backward" formulation the signals from the high-energy particles correspond to the CSW wave front and ordinarily appear as isolated peaks 50–150 ns in duration (Fig. 1a). Thermal particles ($\varepsilon \lesssim 200$ eV) are also detected. The maxima of these signals fall directly behind the CSW wave front. In the case of forward measurements the ion signals change as the CSW approaches the axis. Only thermal ions were recorded simultaneously with the wave front at large radius (Fig. 1b). The higher energy particles were observed far beyond the CSW (300–600 ns later depending on the initial parameters). We note that closer to the axis (r_1) the ion signals corresponding to the CSW wave front are similar to those observed in backward measurements.

Consider the proton energy distributions. The spectra for particles travelling along the the wave front are shown in Fig. 2. A group of 300–800 eV ions is evident in the distributions measured in the backward mode (curves 1, 2). The distribution section at lower ε corresponds to the thermal tail of the distribution function of the bulk (n) of the particles. Assuming an anisotropic beam and an isotropic core distribution the number of accelerated ions satisfies $n^* \leqslant 0.1\, n$. The distributions at both radii are similar, while the maximum proton energies ε_{max} are comparable. The current spectra (Fig. 2) measured at various radii were different. At a large radius r_2 (curve 3) there were virtually no particles accelerated to high energies. The ion energies were less than 200–300 eV. Particles of 300–600 eV appeared when the CSW reached $r_1 = 3$ cm (curve 4). The energy spectra corresponding to current signals far behind the CSW wave front were identical at both radii.

2.2. Measurements normal to the wave front plane

Reflected ions of energies $\varepsilon_{ref} \lesssim 4\varepsilon_n$ where $\varepsilon_n = MU^2/2$ (U is the velocity of radial motion of the potential jump at the CSW) were observed in radial measurements (normal to the wave front). Protons with energies of up to 900 eV leading the CSW were recorded in the case $n_0 \gtrsim 4\cdot 10^{13}$ cm^{-3} ($B_0 = 212$ G, Fig. 3), i.e., $\varepsilon \sim \varepsilon_{ref}$. In the case $n_0 < 4\cdot 10^{13}$ cm^{-3} (Fig. 4) the peak of the high energy particles $\varepsilon \lesssim 4\varepsilon_n$, in addition to the thermal ions, also appears at the wave front.

Standard ion energy distributions reflecting the evolution of the distributions from intersection of the CSW are shown in Figs. 3 and 4. The beam spectra are recorded at high initial concentrations in front of the wave front (Fig. 3, curve 1). The distributions are approximated by Maxwellian distributions at and behind the wave front (curves 2, 3). In the case of n_0 the spectra differ from thermal spectra both in front of and at the wave front (Fig. 4, curves 1–3). Relaxation to a Maxwellian distribution occurs behind the CSW wave front (curve 4).

2.3. Measurements at an angle to the CSW plane

The signal structure at a 35° angle of observation to the normal in the r–φ plane (the current plane) was identical to the signal structure in the radial measurement case. No high energy particles were found at 45° to the normal in the r–z plane across the entire range of initial parameters.

In addition to the "radial" distributions (curve 1) and the distributions along the wave front in both the forward and backward formulations (Fig. 6, spectra 5,4) Figs. 5 and 6 also provide the distributions for protons travelling at 35° to **n** in the backward formulation (curve 2) and the forward formulation (3). In front of the CSW wave front the energies

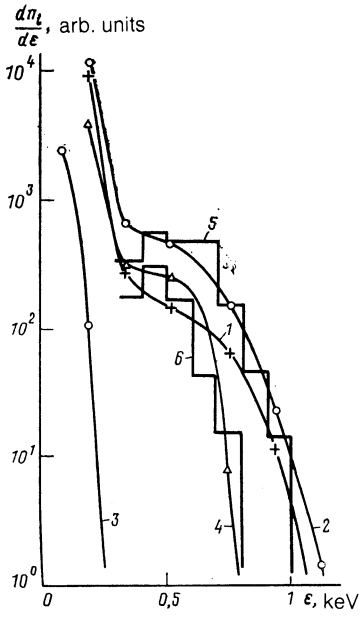

FIG. 2. Energy distributions of ions travelling along the wave front: 1, 2, 5—backward; 3, 4, 6—foreward; 1, 3—$r_2 = 6$ cm; 2, 4–6—$r_1 = 3$ cm; 5,6—numerical calculation.

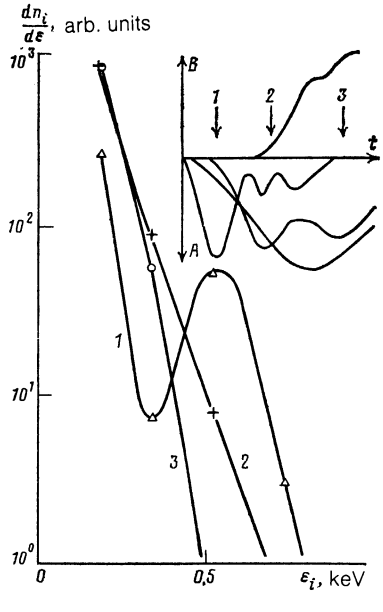

FIG. 3. Ion energy distributions for radial intersection of the CSW (curves 1–3) and standard signals from a magnetic probe $B(t)$ and several energy analyzer channels (accounting for transit time) $A(t)$; $n_0 \gtrsim 4\cdot 10^{13}$ cm^{-3}, $B_0 = 212$ G.

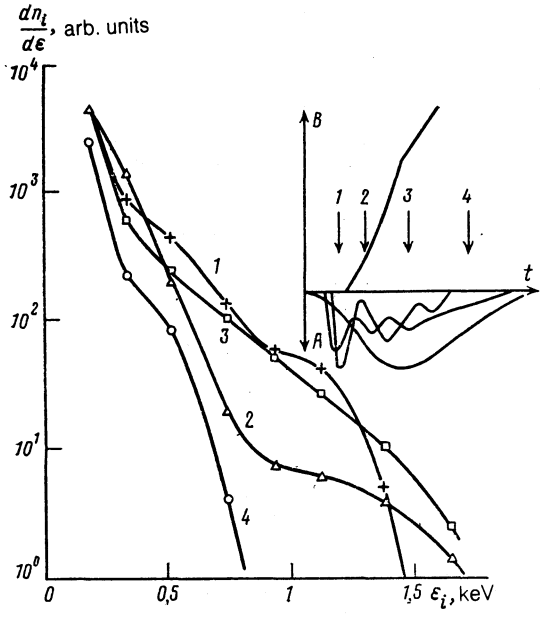

FIG. 4. Ion energy distributions for the case of radial intersection of the CSW (curves 1–4) and typical signals from a magnetic probe $B(t)$ at several energy analyzer channels (accounting for transient time) $A(t)$; $n_0 < 4 \cdot 10^{13}$ cm^{-3}, $B_0 = 212$ G.

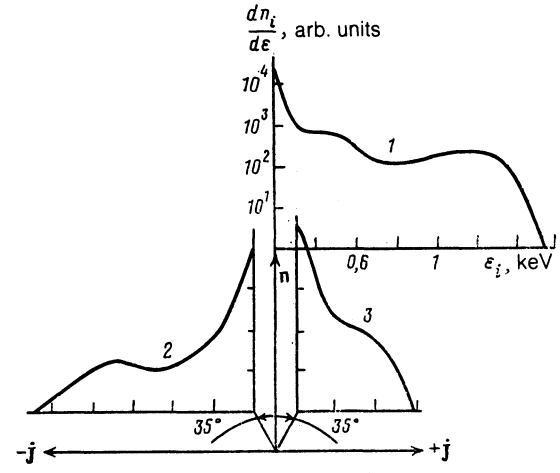

FIG. 5. Ion energy distributions in front of the CSW wave front for the radial direction (curve 1) and at a 35° angle in the backward (curve 2) and the forward direction (curve 3); $B_0 = 212$ G, $U = 2.5 \cdot 10^7$ cm/s.

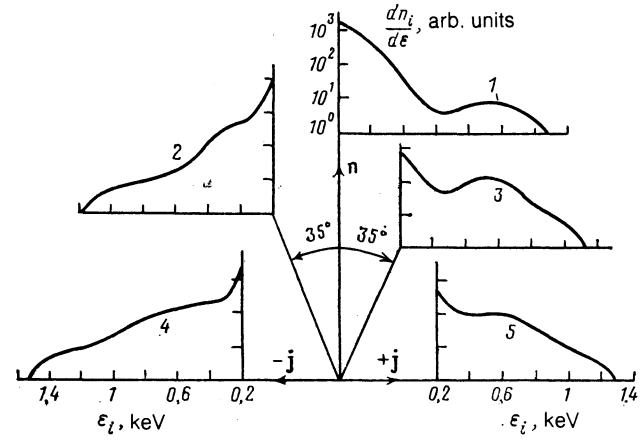

FIG. 6. Ion energy distribution at the CSW wave front for 0° and 35° (curves 1–3), along the wave front in the backward direction (4) and forward direction (5); $B_0 = 212$ G, $n_0 \approx 2 \cdot 10^{13}$ cm^{-3}.

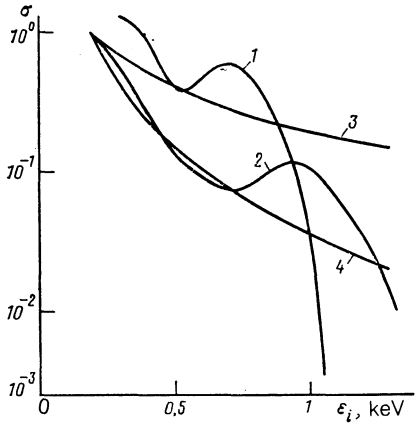

FIG. 7. The "scattering cross-section" σ plotted as a function of ion energy (in front of CSW wave front). Curve 1—$\alpha = 35°$, forward; 2—$\alpha = 35°$, backward. For comparison: 3—$\sigma \propto \varepsilon^{-1}$, 4—$\sigma \sim k/\varepsilon^2$; $B_0 = 212$ G, $U \approx 2.5 \cdot 10^7$ cm/s.

of particles travelling at a 35° angle are less than the "radial" energies, while at the wave front these energies are approximately identical. We note that no protons travelling along the front were detected in front of the CSW.

Assuming that radial emission is the particle source at the 35° angle, Fig. 7 shows the change in the quantity characterizing the effectiveness of reflected proton deflection from the direction $\alpha = 0°$, the "scattering cross-section"

$$\sigma = \frac{dn_i}{d\varepsilon}\Big|_{\alpha=35°} \Big/ \left(\frac{dn_i}{d\varepsilon}\Big|_{\alpha=0°}\right)$$

for the ion signal leading the CSW (corresponding to the spectra in Fig. 5). In the forward formulation σ drops sharply at $\varepsilon \gtrsim 900$ eV, while in the backward formulation the relation is smoother.

A comparison of the maximum recorded energies also provides information on the relationship between ion beam in different directions. It was established that while $\varepsilon_{max} \approx 4\varepsilon_n$ holds in the radial direction and at a 35° angle for all $M_A = U/V_A$ (where $V_A = B_0/(4\pi n_0 M)^{1/2}$) it varies within the range $\varepsilon_n \leqslant \varepsilon_{max} \leqslant 6\varepsilon_n$ along the wave front (Fig. 8). The plot of the curves $\varepsilon_{max} = f(U)$ likewise does not coincide with changing wave velocity (Fig. 9). Moreover Fig. 5 clearly indicates that the signals from the radial direction and the 35° direction are also observed when no ions travel along the wave front. These data suggest that the particle acceleration process along the CSW wave front occurs independent of the reflection and scattering of ions through an angle of 35°.

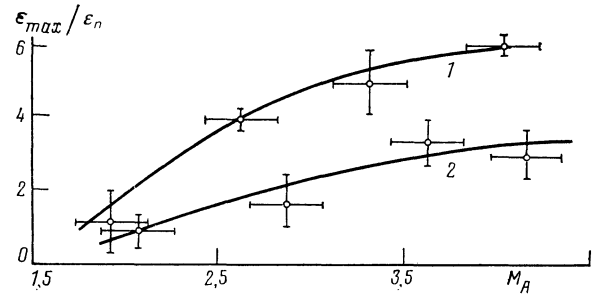

FIG. 8. Plot of the ratio of the maximum recordable energy ε_{max} to the normal energy ε_n for various Mach numbers $r = 3$ cm: Direction: backward. Curve 1—$B_0 = 310$ G, 2—$B_0 = 212$ G.

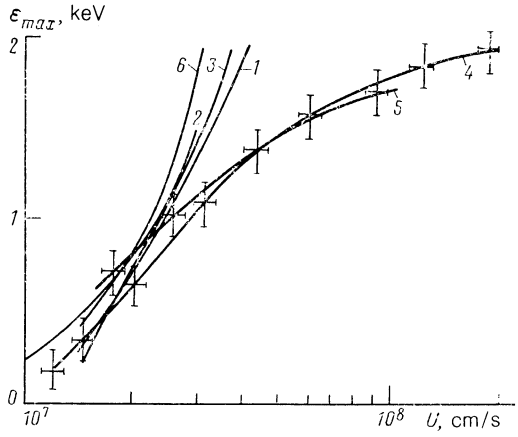

FIG. 9. Maximum detectable energy ε_{max} plotted as a function of CSW velocity: 1—Radial direction, 2—35°, backward, 3—35°, forward 4—r_1 measured along the wave front: Backward, 5—r_1 measured along the wave front, forward, 6—$\varepsilon = M(2U)^2/2$.

The results from potential measurements at the CSW are shown in Fig. 10. Two isomagnetic jumps are observed in the profile of the potential probe signals; these jumps approach one another with decreasing density (increasing velocity U). The first jump is found at the CSW pedestal, while the second is behind or at the wave front.

3. DISCUSSION OF RESULTS

An analysis of the energy spectra measured along the CSW wave front demonstrates that the ions observed here travel with the wave converging on the axis. The Larmor radius of the energetic particles exceeds the radius of the device and hence the radial electrical field at the CSW plays the primary role in ion capture.

In the single-particle approximation the motion of such particles is determined by forces acting in the radial direction and the law of conservation of the azimuthal moment. It is possible to obtain an estimate of the maximum azimuthal velocity from the radial particle equilibrium at an orbit of radius r:

$$V_\varphi \leqslant \left(\frac{r^2\omega_B^2}{4} + c\omega_B r\frac{E_r}{B_z}\right)^{1/2} \pm \frac{r\omega_B}{2} \qquad (1)$$

(the " + " sign is for forward particles (in the direction of Larmor rotation), while " − " refers to the backward particles), where $\omega_W = eB_z/Mc$, E_r and B_z are the maximum values of the magnetic and radial electrical fields. The velocity of a particle travelling from r_2 to r_1 and conserving the azimuthal moment satisfies

$$V_{\varphi 1} = V_{\varphi 2}\frac{r_2}{r_1} + \frac{e\Delta\Phi}{2\pi M c r_1}. \qquad (2)$$

Here the first term describes the change in velocity in zero magnetic field, while the second term is associated with the change in magnetic flux $\Delta\Phi$ along the particle trajectory producing the electrical field $E\varphi$ in the direction opposite the current. Expression (2) can be used to obtain ion energy estimates that are in satisfactory agreement with the maximum energies in spectra 1, 3, and 4 in Fig. 2. The measured energies are substantially lower than the energies calculated on the inner chord for backward ions (Fig. 2, spectrum 2) since the trapping condition (1) for these particles is violated as the CSW goes from r_2 to r_1. New particles are attracted to the acceleration state over time $t \sim (0.1\text{–}0.3)\ T_W$ (where $T_W = 2\pi/\omega_W$). The rate of acceleration of backward protons is $d\varepsilon/dt \sim (2\text{–}4)\cdot 10^9$ eV/s.

The second term in equation (2) corresponds to resonant interaction of the ions with the potential jump. The maximum velocity provided by this mechanism in the plane case is $V_p = cE_r/B_z$. The maximum particle energies in the experiment are (0.3–0.9) $MV_p^2/2$. A numerical calculation of the ion acceleration process was carried out in cylindrical geometry for initial parameters corresponding to the experimental parameters in accordance with Eq. (2) and the equation

$$\frac{dV_r}{dt} = \frac{V_\varphi^2}{r} + \frac{e}{M}E_r + \frac{eB_z}{Mc}V_\varphi. \qquad (3)$$

The calculation results are provided in Fig. 2 as histograms for an initial isotropic Maxwellian distribution with an ion temperature of 40 eV and typical $B_z(r)$ and $E_r(r)$ profiles. Satisfactory agreement between calculated and experimental spectra reveals that the acceleration mechanism in regular electrical and magnetic fields associated with CSW accounts for the observed proton acceleration efficiency.

The ion signals behind the CSW wave front (Fig. 1b) lag by $t \approx T_W/2$ the signals corresponding to the wave front for $B_z = B_0 + \Delta B$, where ΔB is the magnetic field jump at the wave front. The signals bear information on the acceleration stages when the wave is near the axis. After requiring one-half Larmor gyration in the region behind the CSW wave front the accelerated ions acquire the higher radius.

We will now turn our attention to the reflected particles. The observed ion scattering may be due to the excitation of ion-acoustic electrostatic oscillations in front of the potential jump resulting from ion-ion interaction. When the energy of relative motion of the reflected particles exceeds T_e (at the foot estimated to be $T_e \lesssim 10$ eV and at the wave front $T_e \lesssim 60$ eV), angular beam deceleration and scattering occur simultaneously.[7] Scattering is described by

$$\cos\theta_{max} = \left(\frac{2}{3}\right)^{1/2}\frac{C_s}{V_0},$$

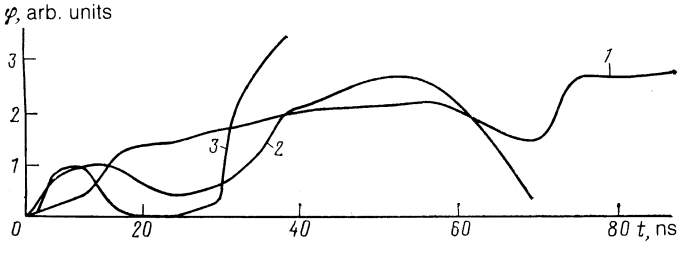

FIG. 10. Potential probe signals ($R_p = 240\ \Omega$) for various angle parameters: 1—$n_0 \approx 1\cdot 10^{14}$ cm^{-3}, 2—$7\cdot 10^{12}$ cm^{-3}, 3—$4\cdot 10^{12}$ cm^{-3}; $B_0 = 310$ G.

where $C_s = (T_e/M)^{1/2}$, V_0 is beam velocity. For the experimental conditions $\theta_{max} \lesssim 80°$. Particles travelling at $\alpha = 35°$ can therefore be attributed to large-angle scattering of particles from the reflected beam in the ion-ion interaction region in front of the CSW wave front. The scattering cross-section drops with increasing proton energy faster than $1/\varepsilon$ for the forward direction and $\sigma \propto 1/\varepsilon^2$ for the "counter-current" direction (Fig. 7). The difference is evidently due to Larmor rotation.

Scattering is more effective at the wave front (see Fig. 6), most likely because the velocities of the reflected ions are comparable to the rising phase velocities of the oscillations. This is possible in the experimental conditions at oscillation wavelengths λ satisfying $10\lambda_D \leqslant \lambda \leqslant 100\lambda_D$, where λ_D is the electron Debye radius. There may be additional scattering by oscillations excited by current flowing at the CSW wave front.

The two peaks of the 35°-reflected particles (at and in front of the CSW wave front) suggests that two scattering regions exist and these regions are determined by two ion beams. These may include ion beams reflected off the two isomagnetic potential jumps (Fig. 10). The potential jumps travel at different velocities and are probably nonstationary. For dimensions $\Delta > \Delta_M$ where Δ_M is the magnetic profile width not only the velocity but also the amplitude and distance between the potential jumps will change. Moreover the first retreating potential jump may be observed yet may not be recorded in identical initial conditions. This phenomenon may have an analogy in the ion beam W-structures observed at the wave front of a near-earth collisionless shock wave.[8]

4. CONCLUSIONS

1. Proton acceleration across a magnetic field and along a CSW wave front was detected experimentally. The substantial difference in the energy of forward and backward particles is attributed to the contribution of the resonant interaction between these particles and the potential jump at the CSW wave front ($U \times B$-acceleration).

2. Two isomagnetic electrostatic potential jumps are observed at the shock wave; these may be associated with the ion interaction regions. Ions reflected at large angles are scattered in the current plane in the vicinity of these jumps.

[1]E. W. Greenstadt, C. T. Russell, J. T. Gosling *et al.*, J. Geophys. Res. **85**, 2124 (1980).
[2]N. A. Strokin, Zh. Eksp. Teor. Fiz., **88**, 2005 (1985) [Sov. Phys. JETP **61**, 1187 (1985)].
[3]R. Z. Sagdeev in: *Reviews of Plasma Physics*, Vol. 4., Ed. by M. A. Leontovich, Consultants Bureau, New York (1966).
[4]V. M. Gubchenko and V. V. Zaitsev, Solar Phys. **63**, 337 (1979).
[5]Y. Ohsawa, Phys. Fluids **28**, 2130 (1985).
[6]S. V. Bulanov and A. S. Sakharov, Pis'ma v ZhETP, **44**, 421 (1986) [JETP Lett. **44**, 543 (1986)].
[7]A. A. Ivanov, S. I. Krashcheninnikov, T. K. Soboleva, and P. N. Yushmanov, Fizika Plazmy **1**, 753 (1975) [Sov. Journal Plasma Physics **1**, 412 (1975)].
[8]V. M. Smirnov and O. L. Vaisberg, Preprint-1301 SRI. Moscow, 1988.

Translated by Kevin S. Hendzel